Analytica Chimica Acta 1073 (2019) 79–89

Contents lists available at ScienceDirect

Analytica Chimica Acta

journal homepage: www.elsevier.com/locate/aca

Investigation of lipidomic perturbations in oxidatively stressed subcellular organelles and exosomes by asymmetrical flow field–flow fractionation and nanoflow ultrahigh performance liquid chromatography–tandem mass spectrometry

Joon Seon Yang, Jin Yong Kim, Jong Cheol Lee, Myeong Hee Moon*

Department of Chemistry, Yonsei University, 50 Yonsei-Ro, Seoul, 03722, Republic of Korea

HIGHLIGHTS

- Oxidative stress effect on lipids of subcellular fractions and exosome is investigated.
- Size and population changes in subcellular fractions and exosome are examined by flow FFF.
- Oxidized phospholipids, TG, and Cer in subcellular fractions and exosome showed different patterns of alteration.
- Flow FFF and nUHPLC-ESI-MS/MS can be a powerful method to analyze lipidomic perturbation in cellular components.

GRAPHICAL ABSTRACT

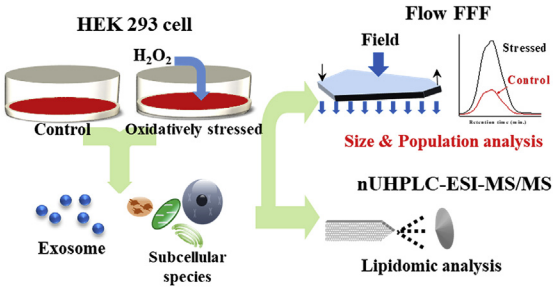

ARTICLE INFO

Article history:
Received 18 January 2019
Received in revised form
23 April 2019
Accepted 27 April 2019
Available online 1 May 2019

Keywords:
Oxidative stress
Lipidomic alteration
Organelle
Exosome
Flow field–flow fractionation
nUHLC-ESI-MS/MS

ABSTRACT

We investigated the effect of oxidative stress (OS) on lipidomic perturbations in the subcellular fractions and exosomes of human embryonic kidney (HEK) 293 cells using asymmetrical flow field–flow fractionation (AF4) and nanoflow ultrahigh performance liquid chromatography–electrospray ionization –tandem mass spectrometry (nUHPLC-ESI-MS/MS). We treated HEK 293 cells with hydrogen peroxide (H_2O_2) and fractionated the cell lysates using AF4 to determine the change in size and population of the subcellular fractions and exosomes, and to obtain narrow size fractions for lipid analysis. A total of 438 lipids from 642 identified species—including oxidized lipids—were quantified. The relative amount of secreted exosomes increased by 28% during OS, whereas the amount of subcellular species decreased by 35%. There was a significant increase in the level of oxidized phospholipids in the mitochondrion-enriched subcellular fractions, but not in the exosomes. Most high-abundance triacylglycerol (TG) species increased in the stressed cells, whereas they decreased in the exosomes. During OS, ceramides involved in the apoptotic mitochondrial pathway were accumulated in the subcellular fractions, whereas their levels were unaffected in the exosomes. The present study demonstrated that AF4 and nUHPLC-ESI-MS/MS can be used to investigate lipid alterations in subcellular and extracellular species during OS, and the pathological relationships in diseases caused by reactive oxygen species.

* Corresponding author.
E-mail address: mhmoon@yonsei.ac.kr (M.H. Moon).

https://doi.org/10.1016/j.aca.2019.04.069
0003-2670/

1. Introduction

Oxidative stress (OS) is defined as a perturbation in the balance between the production of reactive oxygen species (ROS) and the protective capacity of antioxidants, which causes damage to lipids, proteins, and DNA [1–3]. ROS such as the hydroxyl radical (·OH), the superoxide anion (O_2^-), and hydrogen peroxide (H_2O_2) are produced as by-products of biochemical processes, or from oxidizing pollutants such as ozone or nitrogen dioxide, but also act as signalling molecules to regulate physiological functions [2]. Because OS is closely associated with several lifestyle diseases such as atherosclerosis [4], diabetes [5], cancer [6], and neurodegenerative diseases (Alzheimer's and Parkinson's disease) [7], numerous researchers have attempted to identify biomarker candidates of ROS and to elucidate the pathological relationships of diseases.

The generation of ROS and their removal by antioxidants are closely associated with subcellular organelles. Mitochondria produce superoxide anions as a by-product of oxidative phosphorylation through the single electron reduction of O_2, whereas the mitochondrial outer membrane generates membrane-permeable H_2O_2 by dismutation and also releases enzymes such as glutathione peroxidase 4 (GPX4) to remove ROS [8–10]. The endoplasmic reticulum (ER) is a specialized membrane-bound organelle that is involved in oxidative protein folding caused by the production of ROS and is related to redox homeostasis [11]. Peroxisomes not only produce peroxisomal oxidase-derived ROS but also provide protection from OS via strong ROS disposal enzymes such as catalase [12]. Therefore, subcellular organelles are deeply involved in generating and scavenging ROS. Once the balance of the cell redox state has been disturbed by external ROS or other factors, OS can also occur. Exosomes, extracellular vesicles of 30–100-nm diameter, are secreted from cells and are not known to produce ROS directly or participate in the redox mechanism. However, during OS they transmit protective signals by transferring mRNA or phosphoproteins to recipient cells [13,14].

OS in cells has been known to damage proteins, mRNA, DNA, and lipids. In particular, the oxidation of lipids by ROS typically occurs with phospholipids (PLs), in which oxidation begins with the insertion of oxygen into the double bond of the fatty acyl chain, generating a hydroperoxy radical that is further reduced to form various types of oxidized phospholipids (Ox-PLs): PLs with hydroxy, keto, and hydroperoxy groups on the unsaturated fatty acyl chain; PLs with shortened or cleaved acyl chains, etc. [15,16]. Ox-PLs in the plasma membrane bilayer cause alterations in membrane fluidity and permeability [17]. Ox-PLs are an important cause of atherosclerosis because they stimulate the aggregation of platelets during the oxidation of low-density lipoproteins (LDL) in the blood and are associated with inflammatory diseases [18,19]. Complicated Ox-PL structures have been studied using liquid chromatography with electrospray ionization–tandem mass spectrometry (LC-ESI-MS/MS) [20,21], including the Ox-PLs in LDL [22,23], oxidatively stressed cells [24], and modified liposomes [25,26]. However, there have been few investigations on the influence of OS on lipid oxidation in specific organelles such as mitochondria and peroxisomes. The lipid oxidation profiles of exosomes under OS have not been elucidated, although alterations in mRNA content and the levels of phosphoproteins have recently been reported [13,14]. A recent study showed that the size and size distribution of human urinary exosomes from patients with prostate cancer increase with significant changes in lipid profiles [27]. Therefore, the influence of OS on the quantity of subcellular species, the secreted number of exosomes, and the systematic changes in the degree of lipid oxidation is an interesting topic of research. A selective method is required to isolate or purify subcellular and extracellular species from cells. Organelles are isolated by traditional centrifugation methods or affinity-based purification. However, these two techniques have limitations: traditional centrifugation requires the use of a high-density solution that ultimately needs to be removed [28,29], and affinity-based purification requires organelle-specific antibodies or fluorescent proteins [30,31].

Asymmetrical flow field–flow fractionation (AFlFFF or AF4) is an elution-based separation method for the size-dependent fractionation of nano-to micron-sized particles and macromolecules [32,33]. AF4 separation is achieved in an empty rectangular channel space by utilizing the interaction between two flow streams: a migration flow directed along the channel axis to drive sample components toward a detector, and a crossflow moving across the thin flat channel. When particles are pushed toward the channel wall by the crossflow, they migrate along the channel at different velocities depending on their size. Small particles diffuse faster while they are being pushed toward the channel wall by the crossflow, and their diffusional layer against the channel wall becomes thicker than that of larger particles, whose layer becomes more compact due to the slow diffusion. Therefore, the size-based separation of sample components in AF4 is achieved according to the increasing order (normal mode) of the hydrodynamic diameters or molecular weights of the submicron-sized species [34]. However, typically the diffusion of particles or cells larger than 1 μm is negligible. Therefore, particle separation in this size range is achieved according to decreasing order (steric/hyperlayer mode) of diameter because the degree of exposure of the particles to a higher stream velocity of migration flow will be greater for the larger particles. Because AF4 utilizes biocompatible buffer solutions and provides narrow size fractions of sample components for secondary analysis, it has been widely used for various biological materials, including proteins [35], protein aggregates [36], cells [37], bacteria [38], lipoproteins [39], virus-like particles [40], subcellular species [41], and exosomes [27].

In the present study, we investigated the effect of OS on the size, population, and lipid distribution of subcellular species and exosomes from human embryonic kidney (HEK) 293 cells using AF4 and nanoflow ultrahigh performance liquid chromatography–electrospray ionization–tandem mass spectrometry (nUHPLC-ESI-MS/MS). We induced OS in the HEK293 cells by incubating them with H_2O_2. Cell homogenates containing subcellular species were size-sorted using the steric/hyperlayer mode, and exosome extracts were size-sorted using the normal mode of AF4. During the separation of the cell homogenate, we collected subcellular fractions with a narrow size distribution to investigate quantitative changes in lipids including Ox-PLs under OS using nUHPLC-ESI-MS/MS. The present study demonstrates that the combination of AF4 and LC-MS/MS is a powerful technique for the high-speed separation of subcellular species and for the study of lipidomic alterations in subcellular and extracellular species during OS.

2. Materials and methods

2.1. Materials and reagents

We purchased the following chemicals from Sigma-Aldrich (St. Louis, MO, USA): low density lipoprotein (LDL) standard, 2′,7′-dichlorodihydrofluorescein diacetate (H_2DCFDA), 4-(2-hydroxyethyl)-1-piperazineethanesulfonic acid (HEPES), $MgCl_2$, KCl, dithiothreitol (DTT), cOmplete™ mini ethylenediaminetetraacetic acid (EDTA)-free protease inhibitor cocktail, methyl *tert*-butyl ether (MTBE), 0.4% trypan blue solution, and 3% H_2O_2 solution. Trypsin-EDTA; polystyrene (PS) standards with nominal diameters of 46 nm, 102 nm, 203 nm, 1.999 μm, 4.000 μm, and

6.007 μm (hereafter referred to as 50 nm, 100 nm, 200 nm, 2 μm, 4 μm, and 6 μm) were purchased from Thermo Fisher Scientific (Waltham, MA, USA). We acquired HPLC-grade water, acetonitrile (ACN), isopropanol (IPA), and methanol (MeOH) for nUHPLC-ESI-MS/MS analysis from J.T. Baker Inc. (Phillipsburg, NJ, USA). NH_4HCO_2, NH_4OH, and $CHCl_3$ were purchased from Sigma-Aldrich (St. Louis, MO, USA). A total of 15 lipid standards used for the optimization of nUHPLC-ESI-MS/MS experiments were purchased from Avanti Polar Lipid Inc. (Alabaster, AL, USA): lysophosphatidylcholine (LPC) 17:0, phosphatidylcholine (PC) 13:0/13:0, lysophosphatidylethanolamine (LPE) 17:1, phosphatidylethanolamine (PE) 17:0/17:0, lysophosphatidylserine (LPS) 17:0, phosphatidylserine (PS) 17:0/20:4, phosphatidylinositol (PI) 17:0/20:4, lysophosphatidic acid (LPA) 17:0, phosphatidic acid (PA) 17:0/17:0, lysophosphatidylglycerol (LPG) 17:1, phosphatidylglycerol (PG) 15:0/15:0, sphingomyelin (SM) d18:1/17:0, ceramide (Cer) d18:1/17:0, hexosylceramide (HexCer) d18:1/17:0, and D_5-triacylglycerol (TG) 17:0/17:1/17:0. We used 15 lipid standards with odd-numbered acyl chains as internal standards (ISs) as listed in Table S1.

2.2. Cell culture, induction of oxidative stress, viability test, and ROS detection

We obtained human embryonic kidney cell line 293 (HEK293) cells from the Korean Cell Line Bank (Seoul, Republic of Korea). The cells were cultured with minimum essential medium (MEM) from Thermo Fisher Scientific with 10% exosome-depleted heat-inactivated foetal bovine serum (FBS) from System Bioscience, LLC. (Palo Alto, CA, USA), 1% penicillin–streptomycin, and non-essential amino acid supplements in 100-mm culture dishes at 37 °C in an incubator with 5% CO_2. When approximately 90% cell confluency was reached (within 72 h), subculture was performed by adding 0.25% trypsin-EDTA. To induce OS, we added H_2O_2 (5, 10, 25, 50, and 100 μM) 24 h after subculture, then cultured the cells for a further 72 h. For the viability test, we mixed 100 μL of the cell suspension with 100 μL of 0.4% trypan blue staining solution for 2 min, then counted the stained and non-stained cells using a haemocytometer from INCYTO (Cheonan, Republic of Korea). The cellular ROS level was determined using H_2DCFDA according to the following procedures. The HEK293 cells (approximately 1.0×10^4 cell/mL) were treated with a specific concentration of H_2O_2 and then cultured in a 96-well plate. After 72 h, the culture medium was removed and the remaining cells were incubated with 50 μL of 75 μM H_2DCFDA for 30 min in the dark at 37 °C. We washed the incubated cells with 0.1 M phosphate-buffered saline (PBS) solution and measured the fluorescence intensity at 480/545 nm using an Infinite® 200 PRO plate reader from Tecan Ltd. (Zürich, Switzerland).

2.3. Cell homogenization and exosome isolation

We prepared cell homogenate samples containing equal numbers (~8×10^6 cell/mL) of control and oxidatively stressed cells based on the cell counts. The detached cells were centrifuged at 300×*g* for 5 min to remove trypsin-EDTA, washed twice with 0.1 M PBS, then centrifuged at 300×*g* for a further 5 min. We diluted the cell pellets to 4 mL with a hypotonic lysis buffer containing 10 mM HEPES (pH 7.9), 1.5 mM $MgCl_2$, 10 mM KCl, 0.5 mM DTT, and cOmplete™ mini EDTA-free protease inhibitor cocktail, and incubated the mixture at 4 °C for 5 min. We then transferred the mixture to a 7-mL Dounce homogenizer from Wheaton Industries Inc. (Millville, NJ, USA). After 30 strokes with a tight pestle, the homogenate was centrifuged at 15,000×*g* for 10 min, and 50 μL of the supernatant was injected into the FlFFF channel for organelle separation [41].

We isolated exosomes from the culture media of both the control and oxidatively stressed cells. For each group, the culture media from the three flasks (approximately 30 mL) were pooled together. Each culture medium was centrifuged at 3000×*g* for 5 min to remove cell debris, and the supernatant was centrifuged at 12,000×*g* for a further 15 min at 4 °C. We then treated the final supernatants using one of the following three isolation methods: ultracentrifugation (UC) alone, 8% polyethylene glycol (PEG)-aided isolation, or 8% PEG-aided isolation with UC. For UC, we centrifuged the final supernatant in a UC tube at 120,000×*g* and 4 °C for 70 min using an Optima LE-80K Ultracentrifuge equipped with a Type 70 Ti rotor from Beckman Coulter Inc. (Brea, CA, USA). We then removed the supernatant liquid and dispersed the remaining exosome pellet in 200 μL of 0.1 M PBS solution. For PEG-aided isolation, we mixed each supernatant medium with an equivalent volume of 16% PEG solution (Mn = 6000 g/mol from Sigma-Aldrich) to produce a final PEG concentration of 8%. We then stored the mixture for 12 h at 4 °C and centrifuged it at 12,000×*g* for 30 min. The resulting pellet was dispersed in 200 μL of 0.1 M PBS solution for FFF injection. For the third isolation option, we combined the 8% PEG-aided isolation and UC methods according to a procedure described in the literature [42]. The PEG-treated sample was centrifuged at 12000×*g* and the resulting pellet was transferred to a UC tube with 25 mL of 0.1 M PBS solution. We then centrifuged the mixture at 120,000×*g* and 4 °C for 70 min, collected the exosome pellet, and dispersed it in 200 μL of 0.1 M PBS solution. Each exosome sample (50 μL) was injected into the FlFFF channel.

2.4. FlFFF

In the present study, we used a 275-mm long Eclipse LC asymmetrical FlFFF (AF4) channel from Wyatt GmbH (Dernbach, Germany) with a 190-μm-thick mylar spacer (a trapezoidal design with an initial breadth of 2.1 cm and a final breadth of 0.5 cm), and a regenerated cellulose membrane (10-kDa molecular weight cut-off) from Millipore (Danvers, MA, USA). We used a model 7125 injector (50 μL sample loop) from Rheodyne Inc. (Cotati, CA, USA) to inject samples into an AF4 channel. Sample injection was carried out in the focusing/relaxation mode in such a way that the injected sample was focused at a position 1/10 along the channel length at a total crossflow rate of 3.0 mL/min for 5 min. With regard to the AF4 carrier solutions, we used 0.1% FL-70 with 0.02% NaN_3 to separate the PS standards, and a 0.1 M PBS solution for the cell homogenate and exosome samples. All the carrier solutions were made from ultrapure water (>18 MΩ cm) and were filtered through a nitrocellulose membrane filter (0.22-μm pore size) from Millipore. We used a model SP930D HPLC pump from Young Lin Instruments (Seoul, Republic of Korea) to deliver the carrier solutions at an outflow rate/crossflow rate ($\dot{V}_{out}/\dot{V}_c$) = 1.8/1.2 mL/min for the exosomes, and at 2.0/2.5 mL/min for the cell homogenate separations. The eluting materials were detected using a model YL9120 UV/Vis detector at 280 nm, and the detected signals were recorded with Autochro-3000 software, both from Young Lin Instruments. We collected fractions of cell homogenates 10 times in each group (control/stressed) during AF4 separation for lipidomic analysis.

2.5. Lipid extraction

We extracted lipids from the AF4 fractions with MTBE:MeOH using a method adapted from that described by Folch [43]. Before extraction, each AF4 fraction was concentrated to ~200 μL using an Amicon Ultra-15 Centrifugal Filter (30-kDa nominal molecular weight limit) from Millipore, and lyophilized. The dried powder was mixed with 300 μL of MeOH, and the mixture was vortexed briefly and placed in an ice bath for 10 min. We then added 1000 μL of MTBE to the mixture, vortexed for 1 h, added 250 μL of MS-grade

water to the mixture, and vortexed for a further 10 min. The mixture was then centrifuged at 2000×*g* for 5 min. We collected the upper layer in a new 2-mL tube and mixed the remaining aqueous layer with 500 μL of a MeOH:MTBE solvent mixture (3:10, v/v). This process was repeated twice, and the final organic extracts were dried under nitrogen to prevent lipid oxidation using an Evatros mini Evaporator from Goojung Engineering Co. Ltd. (Seoul, Republic of Korea) [44]. Finally, we weighed the dried lipids, reconstituted them in a $CHCl_3$:MeOH solution (1:9, v/v), and further diluted the solution to 5 μg/μL with MeOH:H_2O (8:2, v/v). A mixture of ISs was added to a diluted sample so that the final concentration of each IS was 0.3 pmol/μL.

2.6. nUHPLC-ESI-MS/MS of lipids

We used a Dionex UltiMate 3000 RSLCnano LC system coupled to an LTQ Velos ion trap mass spectrometer from Thermo Scientific™ (San Jose, CA, USA) for the nontargeted identification of lipids. An analytical column was prepared in the laboratory by packing 1.7-μm ethylene-bridged hybrid C18 particles (130 Å) from Waters (Milford, MA, USA) in a pulled-tip capillary column (7 cm × 100 μm, internal diameter). A detailed description of the column preparation can be found in an earlier work [45]. The mobile phase solutions were H_2O/ACN (9:1, v/v) for A and MeOH/ACN/IPA (2:2:6, v/v/v) for B, both of which were added to a modifier mixture (5 mM HCO_2NH_4 and 0.05% NH_4OH) for both positive and negative ion mode detection [46]. For lipid identification with nUHPLC-ESI-MS/MS, we carried out separate runs in positive and negative ion modes. We injected 3 μL of the lipid extract, and carried out sample loading with 99% A for 10 min at 0.9 μL/min. After sample loading, we adjusted the column flowrate to 300 nL/min by splitting the pump flow (7 μL/min) using a 10-port valve. We began gradient elution by ramping the mobile phase B to 60% for 1 min, gradually increasing it to 80% for 10 min, then to 99% for 24 min, and maintaining it at 99% for 5 min. We then reduced it to 1% B and re-equilibrated for 7 min. The ESI voltage was set to 3.0 kV and 40% normalized collision energy was applied for the data-dependent collision-induced dissociation experiments. The mass-to-charge ratio (m/z) range of a precursor MS scan was 350–1100 atomic mass units. We identified the lipids using LiPilot [47] and LipidBlast [48], then confirmed the structures manually.

For targeted lipid analysis, we used a nanoACQUITY UPLC system from Waters coupled with a TSQ Vantage triple-stage quadrupole mass spectrometer from Thermo Scientific™ for the quantitation of lipids based on a selected reaction monitoring (SRM) method. The column and mobile phase solutions were the same as those used for non-targeted identification. Sample loading was performed with mobile phase A at 1 μL/min for 10 min. After loading, the pump flowrate was set to 25 μL/min with a 6-port splitting valve to reduce the column flowrate to 500 nL/min. We began gradient elution by increasing B to 75% for 3 min, then to 100% for 15 min, and maintaining it for 5 min. The pump flow rate was then reduced to 20 μL/min with 100% A within 0.1 min and maintained for 5 min to recondition the column. The various types of precursor ions and quantifier ions selected for different lipid classes are listed in Table S1. The quantification of each lipid was based on its relative peak area compared to that of each IS. Because the concentration of each IS was adjusted to 0.9 pmol per injection, the approximate amount of each lipid can be considered to be the corrected peak area value in pmol. We carried out statistical analysis by the Student's t-test using SPSS software (version 20.0; IBM Corp., Armonk, NY, USA), and principal component analysis (PCA) using the Minitab 17 statistical software package (http://www.minitab.com).

3. Results and discussion

3.1. Oxidative stress in HEK293 cells induced by hydrogen peroxide

We monitored the viability of HEK293 cells during treatment with various concentrations of H_2O_2 by counting the stained cells at different time-points, as shown in Fig. 1a. At 72 h, cell viability remained at or above 80% when the final concentration of H_2O_2 was up to 25 μM. However, it rapidly decreased after 12 h at H_2O_2 concentrations of 50 and 100 μM. The fluorescence measurements represented in Fig. 1b show that the level of ROS increased by more than six times at 25 μM H_2O_2, confirming that 25 μM H_2O_2 was capable of inducing OS in the present study. The number of cells counted after 72 h (Fig. 1c) reveals that the number of oxidatively stressed cells (25 μM H_2O_2) was approximately half that in the control group. Cell growth was possible when a low concentration (3–15 μM) of H_2O_2 was added [49], but the 25 μM H_2O_2 used in the present study inhibited the growth rate of the HEK293 cells.

3.2. FlFFF for subcellular species and exosomes during oxidative stress

We optimized the isolation of exosomes from HEK293 cells before determining exosome distribution during OS using FlFFF. The same amount of cell culture medium was used in the treatment with 8% PEG followed by centrifugation, the treatment by UC alone, and the treatment with 8% PEG and UC, as was used in the washing step [42]. Each resulting pellet was reconstituted to the same volume (200 μL), and 50 μL of each exosome solution was injected into the FlFFF channel. Fig. 2a shows the superimposed fractograms of the exosomes from the control cells using the three different isolation methods. The PS standard particles were separated at the same flow rate condition (outflow rate/crossflow rate ($\dot{V}_{out}/\dot{V}_c$) = 1.9/1.1 mL/min) used for the exosomes. The fractograms in Fig. 2a show that the exosomes were approximately 30–100 nm in diameter, as shown by PS separation in Fig. 2b, which agreed with the results from a previous report on FlFFF [27]. The latter study demonstrated the presence of exosome in the collected fractions using Western blot, therefore, a same confirmation was not carried out. The significant differences in the elution of the three exosome samples in Fig. 2a illustrate that far more exosomes were recovered using the 8% PEG with UC method than with the other two methods. Whereas PEG treatment reportedly results in the presence of unknown impurities and aggregates [50], an additional UC step appears to further purify the exosomes, as evidenced by the complete separation of the void peak at the beginning of the process. In FlFFF, void peaks are usually caused by non-retained low-molecular-weight species in the sample solution. Using the same extraction method, we examined exosome extracts from stressed cells under the same FlFFF run conditions, as shown in Fig. 2b. During OS, the exosomes exhibited similar retention at the peak maximum to the control exosomes, but the peak intensity and area were greater, and the peak distribution was broader. The peak area attributable to exosomes from the stressed cells increased by 28 ± 5% (n = 3), as listed in Table 1, suggesting that exosome secretion increased during OS, which corroborates the results of an earlier study in which more exosomes were released during OS [51]. However, FlFFF analysis of the exosomes revealed a stress-induced increase in exosome size distribution, in which the size limit was increased to an approximate diameter of 130–150 nm based on a comparison with PS separation shown in Fig. 2b.

We investigated subcellular species in the cell homogenates from both the control and stressed cells using the steric/hyperlayer elution mode of FlFFF (Fig. 3) operated at a flow rate condition of $\dot{V}_{out}/\dot{V}_c$ = 2.0/2.5 mL/min. The large particles were eluted earlier

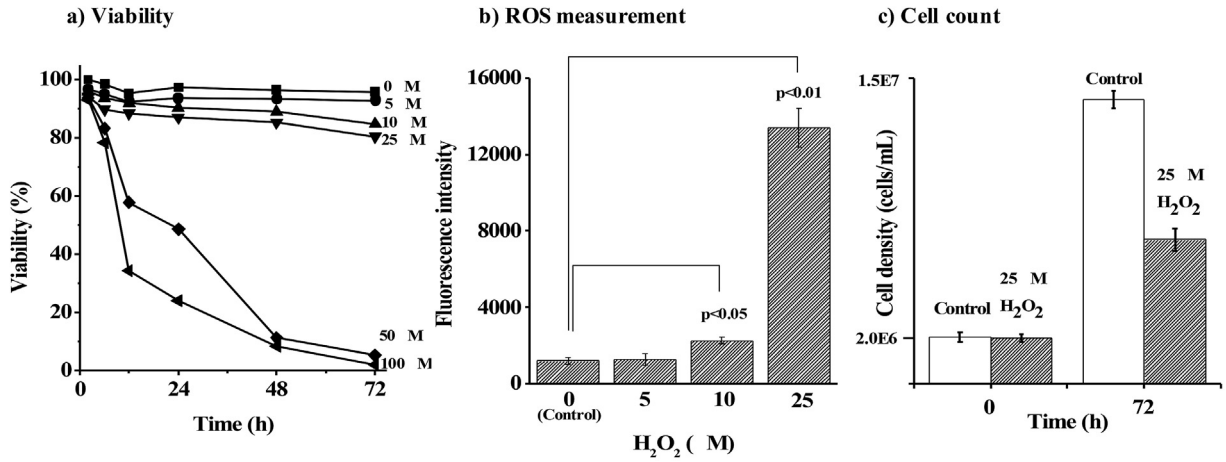

Fig. 1. a) Viability of HEK293 cells tested by varying the concentration of hydrogen peroxide (H_2O_2) in the culture media, b) 2′,7′-dichlorodihydrofluorescein diacetate (H_2DCFDA) assay for the amount of reactive oxygen species (ROS) at various H_2O_2 concentrations based on fluorescence detection, and c) cell counts per mL of control cells and cells treated with 25 μM H_2O_2 after 72 h.

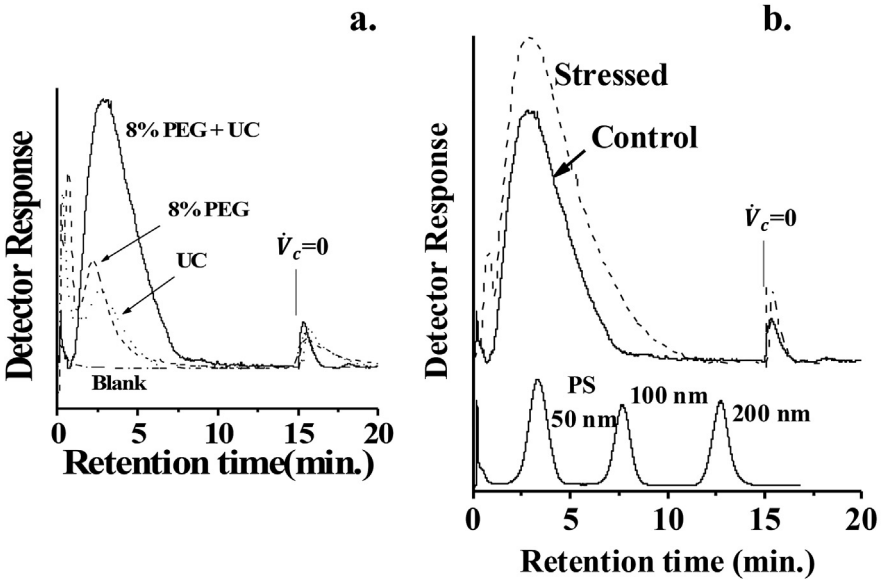

Fig. 2. a) Flow field–flow fractionation (FFF) fractograms of exosome samples obtained by different isolation methods: ultracentrifugation (UC) alone, centrifugation after treating with 8% polyethylene glycol (PEG) overnight, and a combination of the two, b) superimposed fractograms (top) of controls (solid line), exosomes subjected to oxidative stress (dashed line), and polystyrene (PS) standard mixtures (bottom) of nominal diameters 50 nm, 100 nm, and 200 nm. The flow rate conditions were $\dot{V}_{out}/\dot{V}_c$ = 1.9/1.1 mL/min. The crossflow was turned off after 15 min.

than the small ones. Fig. 3 shows the superimposed fractograms for cell homogenates from the control and stressed cells (two repeated runs for each sample), for a blank run, and for PS separation. We carried out the blank run to determine if there was any unwanted adsorption of the sample components at the channel membrane; the peaks at 12 min are nearly the same regardless of sample injection, revealing that there was a system pulse caused by the pressure change when the crossflow was turned off ($\dot{V}_c$= 0). The fractograms of the cell homogenates shown in Fig. 3 are nearly the same as those obtained in an earlier study. We presume that the three prominent peaks in Fig. 3 are attributable to homogenates that contained nuclei and some proteins (F1), mitochondria-enriched fraction (F2), and peroxisome-enriched fraction (F3). Because the elution profile was the same as the previous results which were confirmed with Western blots and nLC-ESI-MS/MS-based proteomic analysis [41]. The three replicate runs of each cell homogenate were carried out by adjusting the injection amount so that there was approximately the same number of cells in the control as in the stressed group. The peak areas of the first peak (F1) were almost the same in both groups. However, there were reproducible reductions in the peak areas of F2 and F3 in the stressed group. The peak area of F2 decreased by 13% ($p = 0.015$ according to the Student's t-test), as shown in Table 1. In contrast,

Table 1
Ratios of peak area values of exosomes in Fig. 2a and each fraction in Fig. 2b.

Fraction	Time (min)	Area ratio (stressed/control) (n = 3)	p-value
Exosome	0.9–11.0	1.28 ± 0.05	<0.01
F1	0.5–3.0	1.01 ± 0.03	0.67
F2	4.0–6.0	0.87 ± 0.11	0.015
F3	6.0–8.5	0.65 ± 0.09	<0.01

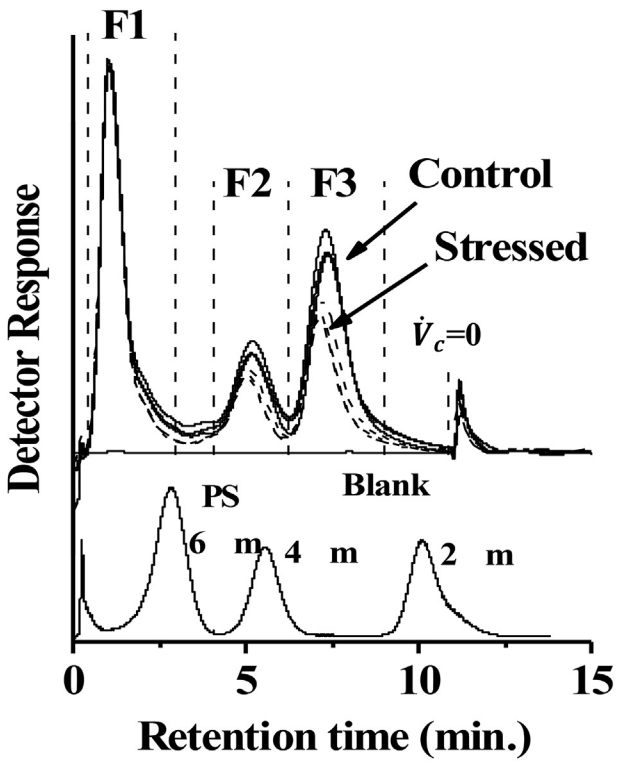

Fig. 3. Superimposed fractograms of cell homogenates (top) from controls (solid line) and oxidatively stressed (dashed line) HEK293 cells including a blank run, and polystyrene (PS) standard mixtures (bottom) of diameters 2 μm, 4 μm, and 6 μm. The flow rate condition was $\dot{V}_{out}/\dot{V}_c = 2.0/2.5\ mL/min$. The crossflow was turned off after 11 min.

the peak area of F3 decreased by 35% ($p < 0.01$). Mitochondria and peroxisomes are the main organelles that dispose ROS produced in the cell. Organelle degradation may be due to the damage caused by H_2O_2 or the need for cellular degradation following the disposal of ROS [52–54]. Whereas the relative amount (approximately number) of exosomes increased during OS, the number of subcellular species decreased. This was further investigated by examining the changes in the amounts of lipids in the fractions during OS.

3.3. Lipidomic changes in subcellular fractions and exosome during oxidative stress

We used nUHPLC-ESI-MS/MS to determine the lipidomic changes in the subcellular fractions (F1–F3) collected during the FlFFF runs, the exosomes, and cells that had been subjected to OS or had received no treatment. Lipid separation was demonstrated by the base peak chromatograms (BPCs) of the lipid standards obtained in both positive and negative ion modes of nUHPLC-ESI-MS/MS, as shown in Supplementary Fig. S1. The BPCs of the lipid extracts from the cells and exosomes are shown in Fig. S2. We determined the molecular structures of the lipids from the data-dependent collision-induced dissociation spectra, which identified 642 lipid species including PLs, sphingolipids (SLs), glycerolipids (GLs), cholesteryl esters (CEs), and Ox-PLs. Among them, 438 species were selected for targeted quantitation by SRM mode. The calculated stressed/control ratio (S/C) of each lipid species in the cells, F1, F2, and F3 fractions, and the exosomes are listed in Table S2, based on the corrected peak area (*vs* that of the IS specific to each lipid class) of each species according to nUHPLC-ESI-MS/MS. The quantified results for PC, PE, and the TG species are expressed as the total number of carbon atoms in the acyl chains and double bonds, because the geometrical isomers of the three lipid classes were not differentiated by SRM quantification. However, the molecular structures of the isomers determined by non-targeted identification are listed in Table S3.

High-abundance PL species were sorted out from the quantified results, and the level change ($\log_2$(S/C)) in each species during OS was compared among the different subcellular fractions in Fig. S3. A high-abundance lipid species was defined as a lipid with a relative abundance higher than 100%/number of lipids within the class. The plots in Fig. S3 are grouped into high abundance lysophospholipids (LPLs)—which are short chain products, saturated, monounsaturated, and polyunsaturated acyl chain types. The $\log_2$(S/C) values of the high abundance LPLs in Fig. S3 increased to some degree, but there were no significant changes in the $\log_2$(S/C) values of the saturated and monounsaturated PLs. However, the $\log_2$(S/C) values of the polyunsaturated species gradually decreased as the number of double bonds increased: the $\log_2$(S/C) values of species with more than five double bonds decreased by more than twofold. This tendency was prominent in subcellular fractions F2 and F3 compared to the others.

Oxidative stress results in the oxidative modification of lipids to produce Ox-PLs. Such modifications include the hydroperoxylation or hydroxylation of unsaturated acyl chains (producing long-chain products (LCPs)); the truncation of acyl chains into shorter chains terminated with either aldehyde or carboxyl groups (producing short-chain products (SCPs)); and the production of LPLs. It is interesting to trace the levels of Ox-PLs, although they are very complicated to monitor thoroughly. We identified a total of 93 Ox-PL species (Table S4); there were 46/29 LCP/SCP species in the stressed cells, and 27/33 species in the control cells. In the exosomes, 40/23 species were found in the stressed condition, whereas 22/24 species were identified in the controls. The number of identified oxidized products increased during OS in both the cells and exosomes, mainly due to the increase in LPCs. Fig. 4 is a plot of the relative amounts of Ox-PLs during OS according to the different polar head groups of the PLs based on a peak area comparison between the total Ox-PLs of each PL class and their corresponding intact PLs. It demonstrates that significant amounts of Ox-PLs were produced during OS in all six PL classes: 2–8 times more than in the controls. Moreover, the relative amounts of oxidized products during OS were much larger in fractions F2 and F3 than in the exosomes, in which the proportion was less than 1%. The degrees of oxidation were found to be larger in PC, PA, and PI than other PL classes, however, reasons for the preferred oxidation are not clear and should be further investigated. Although the plots in Fig. 4 were based on the total peak areas of the identified Ox-PLs, the degrees of hydroxylation or hydroperoxylation in a few high-abundance PL species were calculated. Table 2 shows the S/C ratios of some high-abundance species in the cells, F1, F2, and F3 fractions, and exosomes, and the relative increases in hydroxylation (+O) as RI(OH) and of hydroperoxylation (+OO) as RI(OOH) during OS. The relative increase in hydroxylation, RI(OH), was calculated by taking the increased amount of a specific Ox-PL (e.g. PC 16:0_16:1 + O in Table 2) during stress and dividing it by the amount of intact PL (e.g. PC 32:1). Decreases in the S/C ratio in Table 2 represent decreases in the amount of intact species due to oxidative modification; the S/C ratio decreased to a greater extent in highly unsaturated PL species (e.g. PC 36:5, PE 38:6, and PI 18:0/20:4). These results corroborate those from other studies, demonstrating that lipid peroxidation occurs more readily as the number of double bonds increases [16,55]. The relative increase in hydroxylation was much higher in the F2 and F3 fractions, whereas it did not increase significantly in the exosomes. For instance, the RI value of PE 18:1_22:6 + O was calculated to be 1.73% in the cells, increased to 5.45% in F2 and 10.83% in F3, and was found to be 2.01%

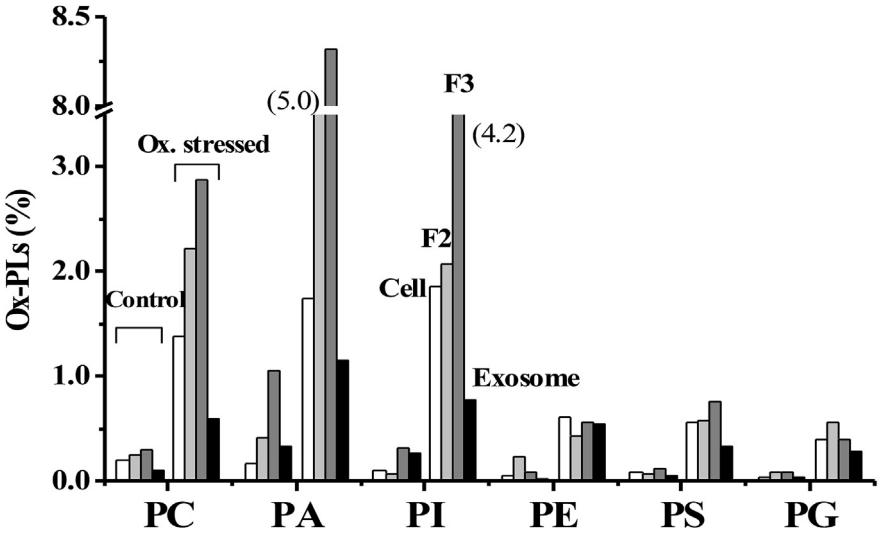

Fig. 4. Relative amounts (%) of oxidized phospholipids (Ox-PLs) in each PL group quantified from different subcellular fractions and exosomes by comparing control cells to cells subjected to oxidative stress.

Table 2
Ratios of stressed/control peak area values (S/C) of intact phospholipids (PLs) and the relative increase (RI) of hydroxylated (RI(OH))) or hydroperoxylated (RI(OOH)) products after oxidative stress compared to the original PL molecule.

Class	Chain	*m/z*		Cell	F1	F2	F3	Exosome
PC	32:1	732.5	S/C[a]	0.78 ± 0.08	0.87 ± 0.15	0.65 ± 0.10	0.73 ± 0.07	0.74 ± 0.07
	16:0_16:1 + O	748.5	RI(OH)[b]	1.50 ± 0.14	0.71 ± 0.43	2.80 ± 0.30	3.59 ± 0.86	1.10 ± 0.30
	36:5	780.5	S/C	0.78 ± 0.10	0.71 ± 0.09	0.54 ± 0.05	0.60 ± 0.12	0.81 ± 0.14
	16:1_20:4 + O	794.5	RI(OH)	3.01 ± 0.52	4.83 ± 3.61	6.46 ± 1.97	4.12 ± 1.13	1.06 ± 0.36
	36:4	782.5	S/C	0.75 ± 0.1	0.62 ± 0.14	0.67 ± 0.06	0.74 ± 0.16	0.93 ± 0.11
	16:1_20:3 + O	798.5	RI(OH)	1.6 ± 1.27	5.7 ± 1.21	6.72 ± 2.21	3.46 ± 3.09	0.58 ± 0.3
	36:3	784.5	S/C	0.82 ± 0.20	0.80 ± 0.19	0.72 ± 0.07	0.86 ± 0.13	0.90 ± 0.22
	18:1/18:2 + O	800.5	RI(OH)	1.2 ± 0.66	1.8 ± 1.99	4.17 ± 1.69	4.57 ± 1.04	0.97 ± 0.3
	36:2	786.4	S/C	0.87 ± 0.08	0.99 ± 0.38	0.83 ± 0.06	0.90 ± 0.22	0.95 ± 0.08
	18:1_18:1 + O	802.5	RI(OH)	0.11 ± 0.03	0.47 ± 0.2	1.6 ± 0.37	2.03 ± 1.29	0.07 ± 0.03
	38:4	810.6	S/C	0.76 ± 0.25	0.88 ± 0.27	0.73 ± 0.07	0.63 ± 0.07	0.96 ± 0.33
	18:0/20:4 + O	826.5	RI(OH)	2.36 ± 2.68	0.86 ± 0.67	2.78 ± 0.42	4.41 ± 1.09	1.47 ± 0.64
PE	36:2	744.5	S/C	0.84 ± 0.05	0.84 ± 0.16	0.80 ± 0.11	0.96 ± 0.09	0.95 ± 0.12
	18:1_18:1 + OO	774.6	RI(OOH)	0.6 ± 0.25	1.18 ± 0.41	1.17 ± 0.3	1.61 ± 1.43	0.26 ± 0.17
	38:6	764.5	S/C	0.53 ± 0.08	0.78 ± 0.12	0.44 ± 0.32	0.46 ± 0.14	0.60 ± 0.09
	16:0_22:6 + OO	794.6	RI(OOH)	2.62 ± 1.13	0.29 ± 0.15	1.28 ± 1.07	3.03 ± 0.82	1.61 ± 0.77
	40:7	790.5	S/C	0.63 ± 0.03	0.48 ± 0.15	0.37 ± 0.15	0.49 ± 0.16	0.51 ± 0.10
	18:1_22:6 + O	806.6	RI(OH)	1.73 ± 0.83	2.86 ± 1.55	5.45 ± 3.17	10.83 ± 2.85	2.01 ± 0.77
PI	18:0/20:4	885.4	S/C	0.44 ± 0.13	0.56 ± 0.24	0.81 ± 0.30	0.49 ± 0.24	0.31 ± 0.07
	18:0/20:4 + O	901.5	RI(OH)	0.59 ± 0.22	1.1 ± 0.33	N.D.	N.D.	0.06 ± 0.19
	18:0/20:3	887.5	S/C	0.54 ± 0.17	0.64 ± 0.10	0.51 ± 0.14	0.57 ± 0.12	0.31 ± 0.17
	18:0/20:3 + O	903.5	RI(OH)	2.62 ± 1.24	2.42 ± 1.43	N.D.	N.D.	1.19 ± 0.73
PG	18:0/16:1	747.5	S/C	0.97 ± 0.13	0.84 ± 0.17	0.81 ± 0.15	0.87 ± 0.37	0.94 ± 0.07
	18:0/16:1 + O	763.5	RI(OH)	1.24 ± 0.6	1.15 ± 0.24	3.75 ± 1.32	4.55 ± 1.42	1.96 ± 0.38
	18:1/18:1	773.5	S/C	0.64 ± 0.14	0.41 ± 0.04	0.64 ± 0.20	0.84 ± 0.23	1.03 ± 0.08
	18:1_18:1 + O	789.5	RI(OH)	5.43 ± 1.11	4.79 ± 0.82	4.03 ± 1.53	2.05 ± 1.57	6.88 ± 1.27
	18:1/22:6	819.5	S/C	0.40 ± 0.11	0.46 ± 0.14	0.32 ± 0.14	0.34 ± 0.18	0.48 ± 0.37
	18:1/22:6 + O	835.5	RI(OH)	2 ± 0.36	16.01 ± 3.09	2.01 ± 1.61	1.75 ± 2.11	7.25 ± 1.49
PA	18:1/20:1	727.5	S/C	1.11 ± 0.37	1.33 ± 0.40	1.48 ± 0.14	1.22 ± 0.68	1.16 ± 0.73
	18:1/20:1 + O	743.5	RI(OH)	0.81 ± 0.19	0.53 ± 1.96	3.4 ± 1.3	5.8 ± 3.56	4.67 ± 1.83

[a] Ratio (S/C) of corrected peak area.
[b] Relative increase of hydroxylated products produced after oxidative stress compared to the amount of the original PL molecule in the control.

in the exosomes. PE is the second most abundant PL in mitochondria and is involved in mitochondrial function [56]. A recent report showed that the PE level decreased significantly in the mitochondria of aged muscle [57]. Because fractions F2 and F3 are enriched with mitochondria and peroxisomes, respectively [41], the increase in Ox-PE species in the two fractions suggests oxidative damage to the mitochondria. However, the Ox-PL levels in the exosomes did not increase as much as expected from the subcellular fractions. This may have occurred because exosomes transfer protective signals to recipient cells during OS [14]. However, the oxidative changes in exosome lipids have not been investigated, and more studies are required to elucidate lipid stability in exosomes during OS. The S/C ratios of PA 18:1/20:1 increased during stress, possibly due to the generation of PA by the dissociation of the polar head

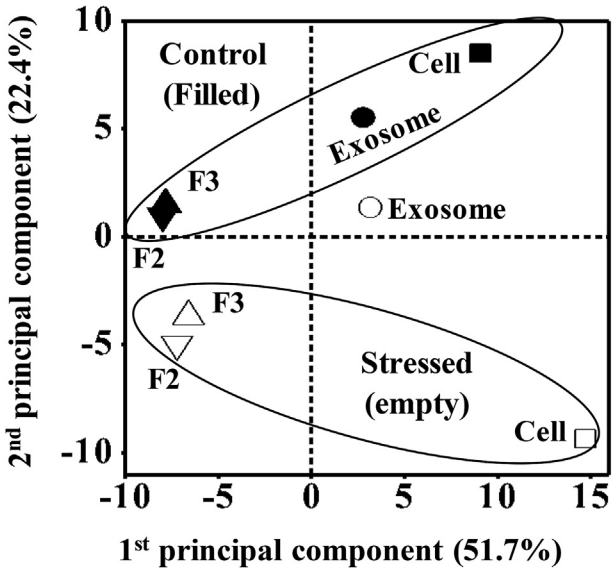

Fig. 5. Principal component analysis (PCA) plots representing the difference before and after oxidative stress at the level of whole cells, F2, F3, and exosomes based on the quantified results for 438 lipids. Data for controls and stressed subjects are represented by filled and open symbols, respectively. Data for whole cells, F2, F3, and exosomes are represented by rectangles, triangles, reversed triangles, and circles, respectively. Filled and open symbols represent controls and stressed subjects, respectively.

groups of other PLs with the same acyl chains. The possibility that the head groups of PL were lost during ESI can be excluded here because lipid quantitation was based on the SRM-targeted detection of molecular ions and quantifier ions at a time interval (±1 min of the retention time), and the retention time of an intact PA is different from that of a PA product derived from in-source fragmentation.

The differences in the overall lipid profiles during OS can be visualized using principal component analysis (PCA) plots obtained for all the quantified lipid species (Fig. 5). The plots reveal that there was a significant difference in the level of lipids in the whole cells but there was less change in the exosome lipids. Whereas the levels of most PL species decreased in the cells during OS, as represented in Fig. S3, high-abundance TG species increased by > 1.5-fold in the whole cells, and the four TGs (52:4, 52:3, 54:4, and 54:3) increased by > 3-fold, as shown in Fig. 6. However, the increase in the subcellular fractions was not as great as in the whole cells. The accumulation of TGs due to ROS can induce non-alcoholic liver failure [58] or chronic kidney disease [59]. TG accumulation can also be caused by sterol regulatory element-binding protein 1c (SREBP1c), which regulates fatty acid biosynthesis during OS [60]. Therefore, the observed increase in TG may be attributed to the increased levels of ROS. We expected stimulated TG species to be enriched in the plasma membrane because they increased in the whole cells more than in the subcellular fractions. Although OS did not influence the levels of PLs in the exosomes in the present study, the levels of the four TGs decreased in the exosomes but increased in the whole cells. The authors of a recent study reported that the total TG levels in exosomes decreased by 40% when rat alveolar epithelial (R3/1) cells were treated with H_2O_2 [61]. There is a significant reduction in the TG levels in exosomes isolated from the urine of patients with prostate cancer [27]. These results suggest that decreases in TG levels in exosomes could be a sign of pathogenic development. Plasmalogen species are known to protect cells against damages from OS and its regulation against OS is closely related to peroxisome metabolism [62]. While the overall amount of PE plasmalogen species was not significantly changed upon OS in this study, the fraction F3 that was enriched with peroxisome showed some increases of high abundance PE plasmalogen species (PE p16:0/20:4 and PE p18:0/20:4 by 26–42% with $p < 0.01$) compared to the other fractions (Table S2).

We investigated alterations in the SM and Cer levels by comparing the S/C ratios of individual species sharing a common acyl chain structure (d18:1/xx:x). Fig. 7 shows that Cer species with sn-2 acyl chain types 18:0 and 22:1 increased by > twofold in subcellular fractions F2 and F3, and those with chain types 22:0 and 24:0 increased by 4- and 2.5-fold, respectively, whereas the corresponding changes were not significant in the whole cells (<1.5-fold) and were negligible in the exosomes. Studies have shown that Cer is associated with the activation of a mitochondrial apoptotic pathway, and it becomes more abundant with age, inducing cell apoptosis [63–65]. In the present study, we detected

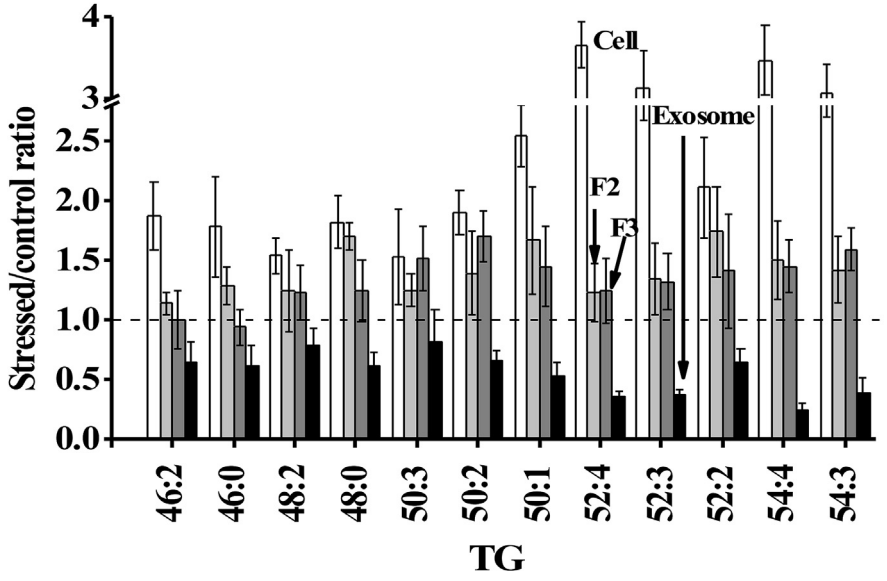

Fig. 6. Ratios of stressed/control peak area values (S/C) of high-abundance triacylglycerol (TG) species in cells, F2, F3, and exosomes.

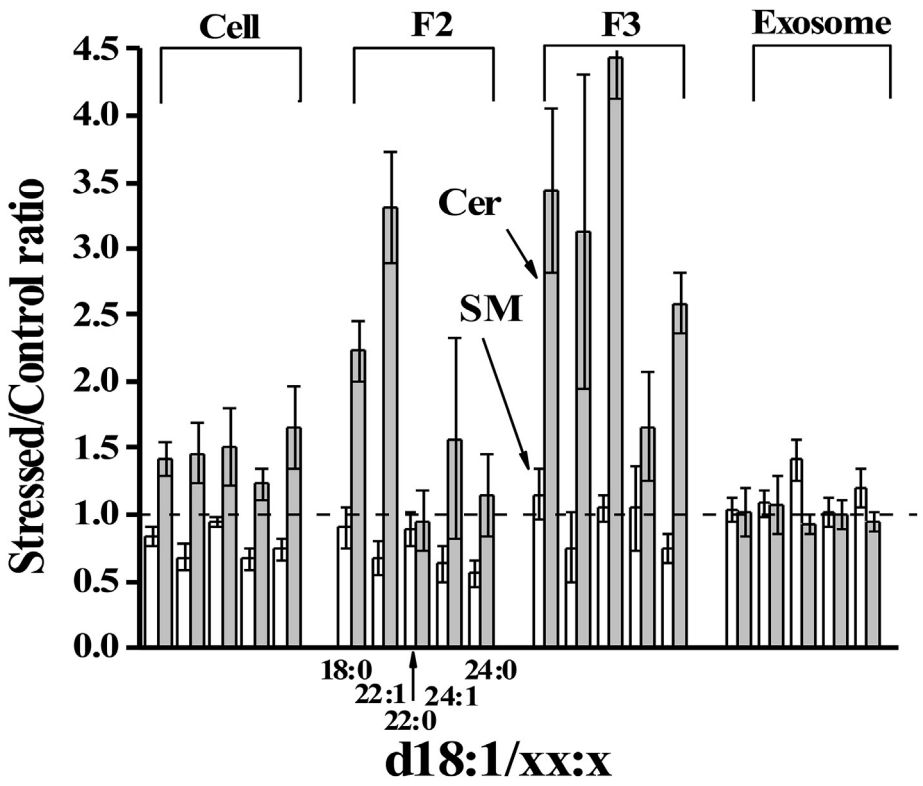

Fig. 7. Ratios of stressed/control peak area values (S/C) of high-abundance sphingomyelin (SM) and ceramide (Cer) species with the same acyl chain based on a d18:1/xx:x structure.

an increase in Cer levels, especially in the F2 and F3 fractions, whereas SM levels decreased to some degree. Moreover, large increases in the levels of Cer in F2 and F3 suggest that OS stimulates the Cer synthesis pathway in mitochondria and peroxisomes. Because Cer can also be produced by the hydrolysis of SM by sphingomyelinase, the increase in Cer levels can be attributed to the substantial decrease in SM. However, the present study demonstrated that Cer levels increased markedly, suggesting that Cer production is probably stimulated by other pathways during OS. The Cer levels in the exosome did not alter significantly, suggesting that during OS exosomes transmit protective signals to recipients through lipids and mRNA [14].

4. Conclusions

The present study demonstrated that an off-line combination of FlFFF and nUHPLC-ESI-MS/MS can be used to study the alterations in size, population, and lipid profiles of subcellular and extracellular species during OS. Treating HEK293 cells with H_2O_2 caused no significant change in the retention times of the peaks attributable to eluted subcellular species, assuming no alteration in the size or size distribution of those species. However, the subcellular species population decreased, whereas the number of secreted exosomes increased during OS. Lipidomic analysis of whole cells, subcellular fractions, and exosomes detected relatively large amounts of oxidized lipids in the mitochondria-enriched fractions, whereas the degree of oxidation in the exosomes was less significant during OS. Among the lipid classes, we found that the levels of most TGs increased in the stressed cells, whereas they were not significant in the subcellular fractions, and even decreased in the exosomes secreted from stressed cells. The reduction in the Ox-PL and TG levels in the exosomes during OS can be regarded as being due to a minimization of their transport to recipient cells, caused by the delivery of protective signals through lipids and mRNA [14]. Moreover, Cer—which is associated with mitochondrial apoptotic pathways—increased by at least 2–3 times in the subcellular fractions containing mitochondria and peroxisomes, suggesting that OS induces an increase in Cer to stimulate apoptosis. The present study demonstrated that size-sorting by FlFFF and lipidomic analysis using nUHPLC-ESI-MS/MS can be used in combination to investigate the influence of OS on the subcellular and extracellular components of cells. The systematic investigation of subcellular species during OS can be achieved once the separation resolution of subcellular species is improved by the stepwise separation of collected fractions in different elution modes, and this warrants further investigation.

Funding

This work was supported by the National Research Foundation (NRF) of the Republic of Korea (grant number NRF-2018R1A2A1A05019794).

Appendix A. Supplementary data

Supplementary data to this article can be found online at https://doi.org/10.1016/j.aca.2019.04.069.

References

[1] D.J. Betteridge, What is oxidative stress? Metab. Clin. Exp. 49 (2000) 3–8.
[2] M. Schieber, N.S. Chandel, ROS function in redox signaling and oxidative stress, Curr. Biol. 24 (2014) R453–R462.
[3] A.M. Pisoschi, A. Pop, The role of antioxidants in the chemistry of oxidative stress: a review, Eur. J. Med. Chem. 97 (2015) 55–74.
[4] U. Singh, I. Jialal, Oxidative stress and atherosclerosis, Pathophysiology 13 (2006) 129–142.
[5] I.C. West, Radicals and oxidative stress in diabetes, Diabet. Med. 17 (2000) 171–180.

[6] V. Sosa, T. Moline, R. Somoza, R. Paciucci, H. Kondoh, L.L. ME, Oxidative stress and cancer: an overview, Ageing Res. Rev. 12 (2013) 376–390.
[7] K.J. Barnham, C.L. Masters, A.I. Bush, Neurodegenerative diseases and oxidative stress, Nat. Rev. Drug Discov. 3 (2004) 205–214.
[8] C.L. Quinlan, I.V. Perevoshchikova, M. Hey-Mogensen, A.L. Orr, M.D. Brand, Sites of reactive oxygen species generation by mitochondria oxidizing different substrates, Redox Biol. 1 (2013) 304–312.
[9] E.B. Tahara, F.D.T. Navarete, A.J. Kowaltowski, Tissue-, substrate-, and site-specific characteristics of mitochondrial reactive oxygen species generation, Free Radical Bio. Med. 46 (2009) 1283–1297.
[10] P. Cole-Ezea, D. Swan, D. Shanley, J. Hesketh, Glutathione peroxidase 4 has a major role in protecting mitochondria from oxidative damage and maintaining oxidative phosphorylation complexes in gut epithelial cells, Free Radical Bio. Med. 53 (2012) 488–497.
[11] S.S. Cao, R.J. Kaufman, Endoplasmic reticulum stress and oxidative stress in cell fate decision and human disease, Antioxidants Redox Signal. 21 (2014) 396–413.
[12] M. Schrader, H.D. Fahimi, Peroxisomes and oxidative stress, Bba-Mol. Cell Res. 1763 (2006) 1755–1766.
[13] L. Biasutto, A. Chiechi, R. Couch, L.A. Liotta, V. Espina, Retinal pigment epithelium (RPE) exosomes contain signaling phosphoproteins affected by oxidative stress, Exp. Cell Res. 319 (2013) 2113–2123.
[14] M. Eldh, K. Ekstrom, H. Valadi, M. Sjostrand, B. Olsson, M. Jernas, J. Lotvall, Exosomes communicate protective messages during oxidative stress; possible role of exosomal shuttle RNA, PLoS One 5 (2010).
[15] M.R. Domingues, A. Reis, P. Domingues, Mass spectrometry analysis of oxidized phospholipids, Chem. Phys. Lipids 156 (2008) 1–12.
[16] A. Reis, C.M. Spickett, Chemistry of phospholipid oxidation, Bba-Biomembranes 1818 (2012) 2374–2387.
[17] G. Barrera, Oxidative stress and lipid peroxidation products in cancer progression and therapy, ISRN Oncol. 2012 (2012) 137289.
[18] T. Kita, N. Kume, M. Minami, K. Hayashida, T. Murayama, H. Sano, H. Moriwaki, H. Kataoka, E. Nishi, H. Horiuchi, H. Arai, M. Yokode, Role of oxidized LDL in atherosclerosis, Atherosclerosis Vi 947 (2001) 199–206.
[19] J. Adachi, M. Asano, N. Yoshioka, H. Nushida, Y. Ueno, Analysis of phosphatidylcholine oxidation products in human plasma using quadrupole time-of-flight mass spectrometry, Kobe J. Med. Sci. 52 (2006) 127–140.
[20] A. Reis, M.R. Domingues, F.M. Amado, A.J. Ferrer-Correia, P. Domingues, Radical peroxidation of palmitoyl-lineloyl-glycerophosphocholine liposomes: identification of long-chain oxidised products by liquid chromatography-tandem mass spectrometry, J. Chromatogr. B Analyt Technol. Biomed. Life Sci. 855 (2007) 186–199.
[21] J.Y. Lee, S. Lim, S. Park, M.H. Moon, Characterization of oxidized phospholipids in oxidatively modified low density lipoproteins by nanoflow liquid chromatography-tandem mass spectrometry, J. Chromatogr. A 1288 (2013) 54–62.
[22] A. Ravandi, G. Leibundgut, M.Y. Hung, M. Patel, P.M. Hutchins, R.C. Murphy, A. Prasad, E. Mahmud, Y.I. Miller, E.A. Dennis, J.L. Witztum, S. Tsimikas, Release and capture of bioactive oxidized phospholipids and oxidized cholesteryl esters during percutaneous coronary and peripheral arterial interventions in humans, J. Am. Coll. Cardiol. 63 (2014) 1961–1971.
[23] J.Y. Lee, S.K. Byeon, M.H. Moon, Profiling of oxidized phospholipids in lipoproteins from patients with coronary artery disease by hollow fiber flow field-flow fractionation and nanoflow liquid chromatography-tandem mass spectrometry, Anal. Chem. 87 (2015) 1266–1273.
[24] C.M. Spickett, N. Rennie, H. Winter, L. Zambonin, L. Landi, A. Jerlich, R.J. Schaur, A.R. Pitt, Detection of phospholipid oxidation in oxidatively stressed cells by reversed-phase HPLC coupled with positive-ionization electrospray [correction of electroscopy] MS, Biochem. J. 355 (2001) 449–457.
[25] P. Sala, S. Potz, M. Brunner, M. Trotzmuller, A. Fauland, A. Triebl, J. Hartler, E. Lankmayr, H.C. Kofeler, Determination of oxidized phosphatidylcholines by hydrophilic interaction liquid chromatography coupled to Fourier transform mass spectrometry, Int. J. Mol. Sci. 16 (2015) 8351–8363.
[26] A. Reis, M.R. Domingues, F.M. Amado, A.J. Ferrer-Correia, P. Domingues, Separation of peroxidation products of diacyl-phosphatidylcholines by reversed-phase liquid chromatography-mass spectrometry, Biomed. Chromatogr. 19 (2005) 129–137.
[27] J.S. Yang, J.C. Lee, S.K. Byeon, K.H. Rha, M.H. Moon, Size dependent lipidomic analysis of urinary exosomes from patients with prostate cancer by flow field-flow fractionation and nanoflow liquid chromatography-tandem mass spectrometry, Anal. Chem. 89 (2017) 2488–2496.
[28] C.P. Satori, V. Kostal, E.A. Arriaga, Review on recent advances in the analysis of isolated organelles, Anal. Chim. Acta 753 (2012) 8–18.
[29] N.R. Sims, M.F. Anderson, Isolation of mitochondria from rat brain using Percoll density gradient centrifugation, Nat. Protoc. 3 (2008) 1228–1239.
[30] A. Cossarizza, D. Ceccarelli, A. Masini, Functional heterogeneity of an isolated mitochondrial population revealed by cytofluorometric analysis at the single organelle level, Exp. Cell Res. 222 (1996) 84–94.
[31] H.T. Hornig-Do, G. Gunther, M. Bust, P. Lehnartz, A. Bosio, R.J. Wiesner, Isolation of functional pure mitochondria by superparamagnetic microbeads, Anal. Biochem. 389 (2009) 1–5.
[32] J.C. Giddings, Field-flow fractionation - analysis of macromolecular, colloidal, and particulate materials, Science 260 (1993) 1456–1465.
[33] K.G. Wahlund, J.C. Giddings, Properties of an asymmetrical flow field-flow fractionation channel having one permeable wall, Anal. Chem. 59 (1987) 1332–1339.
[34] P. Reschiglian, M.H. Moon, Flow field-flow fractionation: a pre-analytical method for proteomics, J. Proteomics 71 (2008) 265–276.
[35] A. Litzen, J.K. Walter, H. Krischollek, K.G. Wahlund, Separation and quantitation of monoclonal-antibody aggregates by asymmetrical flow field-flow fractionation and comparison to gel-permeation chromatography, Anal. Biochem. 212 (1993) 469–480.
[36] C.R. Bria, S.K. Williams, Impact of asymmetrical flow field-flow fractionation on protein aggregates stability, J. Chromatogr. A 1465 (2016) 155–164.
[37] P. Reschiglian, A. Zattoni, B. Roda, L. Cinque, D. Melucci, B.R. Min, M.H. Moon, Hyperlayer hollow-fiber flow field-flow fractionation of cells, J. Chromatogr. A 985 (2003) 519–529.
[38] P. Reschiglian, A. Zattoni, B. Roda, S. Casolari, M.H. Moon, J. Lee, J. Jung, K. Rodmalm, G. Cenacchi, Bacteria sorting by field-flow fractionation. Application to whole-cell Escherichia coli vaccine strains, Anal. Chem. 74 (2002) 4895–4904.
[39] S.K. Byeon, J.Y. Lee, S. Lim, D. Choi, M.H. Moon, Discovery of candidate phospholipid biomarkers in human lipoproteins with coronary artery disease by flow field-flow fractionation and nanoflow liquid chromatography-tandem mass spectrometry, J. Chromatogr. A 1270 (2012) 246–253.
[40] L.F. Pease 3rd, D.I. Lipin, D.H. Tsai, M.R. Zachariah, L.H. Lua, M.J. Tarlov, A.P. Middelberg, Quantitative characterization of virus-like particles by asymmetrical flow field flow fractionation, electrospray differential mobility analysis, and transmission electron microscopy, Biotechnol. Bioeng. 102 (2009) 845–855.
[41] J.S. Yang, J.Y. Lee, M.H. Moon, High speed size sorting of subcellular organelles by flow field-flow fractionation, Anal. Chem. 87 (2015) 6342–6348.
[42] M.A. Rider, S.N. Hurwitz, D.G. Meckes Jr., ExtraPEG: a polyethylene glycol-based method for enrichment of extracellular vesicles, Sci. Rep. 6 (2016) 23978.
[43] S.K. Byeon, J.Y. Lee, M.H. Moon, Optimized extraction of phospholipids and lysophospholipids for nanoflow liquid chromatography-electrospray ionization-tandem mass spectrometry, Analyst 137 (2012) 451–458.
[44] J.Y. Lee, J.S. Yang, S.M. Park, S.K. Byeon, M.H. Moon, On-line high speed lipid extraction for nanoflow liquid chromatography-tandem mass spectrometry, J. Chromatogr. A 1464 (2016) 12–20.
[45] J.C. Lee, S.M. Park, I.Y. Kim, H. Sung, J.K. Seong, M.H. Moon, High-fat diet-induced lipidome perturbations in the cortex, hippocampus, hypothalamus, and olfactory bulb of mice, Bba-Mol. Cell Biol. L 1863 (2018) 980–990.
[46] D.Y. Bang, S. Lim, M.H. Moon, Effect of ionization modifiers on the simultaneous analysis of all classes of phospholipids by nanoflow liquid chromatography/tandem mass spectrometry in negative ion mode, J. Chromatogr. A 1240 (2012) 69–76.
[47] S. Lim, S.K. Byeon, J.Y. Lee, M.H. Moon, Computational approach to structural identification of phospholipids using raw mass spectra from nanoflow liquid chromatography-electrospray ionization-tandem mass spectrometry, J. Mass Spectrom. 47 (2012) 1004–1014.
[48] T. Kind, K.H. Liu, D.Y. Lee, B. DeFelice, J.K. Meissen, O. Fiehn, LipidBlast in silico tandem mass spectrometry database for lipid identification, Nat. Methods 10 (2013), 755-+.
[49] M. Gulden, A. Jess, J. Kammann, E. Maser, H. Seibert, Cytotoxic potency of H2O2 in cell cultures: impact of cell concentration and exposure time, Free Radic. Biol. Med. 49 (2010) 1298–1305.
[50] M.Y. Konoshenko, E.A. Lekchnov, A.V. Vlassov, P.P. Laktionov, Isolation of extracellular vesicles: general methodologies and latest trends, BioMed Res. Int. 2018 (2018) 8545347.
[51] S. Atienzar-Aroca, M. Flores-Bellver, G. Serrano-Heras, N. Martinez-Gil, J.M. Barcia, S. Aparicio, D. Perez-Cremades, J.M. Garcia-Verdugo, M. Diaz-Llopis, F.J. Romero, J. Sancho-Pelluz, Oxidative stress in retinal pigment epithelium cells increases exosome secretion and promotes angiogenesis in endothelial cells, J. Cell Mol. Med. 20 (2016) 1457–1466.
[52] I. Kim, S. Rodriguez-Enriquez, J.J. Lemasters, Selective degradation of mitochondria by mitophagy, Arch. Biochem. Biophys. 462 (2007) 245–253.
[53] M. Frank, S. Duvezin-Caubet, S. Koob, A. Occhipinti, R. Jagasia, A. Petcherski, M.O. Ruonala, M. Priault, B. Salin, A.S. Reichert, Mitophagy is triggered by mild oxidative stress in a mitochondrial fission dependent manner, Bba-Mol Cell Res. 1823 (2012) 2297–2310.
[54] E.B. Aksam, B. de Vries, I.J. van der Klei, J.A.K.W. Kiel, Preserving organelle vitality: peroxisomal quality control mechanisms in yeast, FEMS Yeast Res. 9 (2009) 808–820.
[55] J. Assies, R.J. Mocking, A. Lok, H.G. Ruhe, F. Pouwer, A.H. Schene, Effects of oxidative stress on fatty acid- and one-carbon-metabolism in psychiatric and cardiovascular disease comorbidity, Acta Psychiatr. Scand. 130 (2014) 163–180.
[56] G. Tasseva, H.D. Bai, M. Davidescu, A. Haromy, E. Michelakis, J.E. Vance, Phosphatidylethanolamine deficiency in Mammalian mitochondria impairs oxidative phosphorylation and alters mitochondrial morphology, J. Biol. Chem. 288 (2013) 4158–4173.
[57] A.K. Pollard, C.A. Ortori, R. Stoger, D.A. Barrett, L. Chakrabarti, Mouse mitochondrial lipid composition is defined by age in brain and muscle, Aging (Albany NY) 9 (2017) 986–998.
[58] G. Targher, L. Bertolini, S. Rodella, G. Zoppini, G. Lippi, C. Day, M. Muggeo, Non-alcoholic fatty liver disease is independently associated with an increased prevalence of chronic kidney disease and proliferative/laser-treated retinopathy in type 2 diabetic patients, Diabetologia 51 (2008) 444–450.

[59] N.D. Vaziri, K. Norris, Lipid disorders and their relevance to outcomes in chronic kidney disease, Blood Purif. 31 (2011) 189–196.
[60] M. Sekiya, A. Hiraishi, M. Touyama, K. Sakamoto, Oxidative stress induced lipid accumulation via SREBP1c activation in HepG2 cells, Biochem. Bioph. Res. Co. 375 (2008) 602–607.
[61] C.A. Downs, V.D. Dang, N.M. Johnson, N.D. Denslow, A.A. Alli, Hydrogen peroxide stimulates exosomal cathepsin B regulation of the receptor for advanced glycation end-products (RAGE), J. Cell. Biochem. 119 (2018) 599–606.
[62] N.E. Braverman, A.B. Moser, Functions of plasmalogen lipids in health and disease, Biochim. Biophys. Acta 1822 (2012) 1442–1452.
[63] M. Piccinini, F. Scandroglio, S. Prioni, B. Buccinna, N. Loberto, M. Aureli, V. Chigorno, E. Lupino, G. DeMarco, A. Lomartire, M.T. Rinaudo, S. Sonnino, A. Prinetti, Deregulated sphingolipid metabolism and membrane organization in neurodegenerative disorders, Mol. Neurobiol. 41 (2010) 314–340.
[64] S.A. Lightle, J.I. Oakley, M.N. Nikolova-Karakashian, Activation of sphingolipid turnover and chronic generation of ceramide and sphingosine in liver during aging, Mech. Ageing Dev. 120 (2000) 111–125.
[65] N. Sanvicens, T.G. Cotter, Ceramide is the key mediator of oxidative stress-induced apoptosis in retinal photoreceptor cells, J. Neurochem. 98 (2006) 1432–1444.